Development of Velocity Flow Field Measurement Method Around a Vertical Axis Wind Turbine Blade Using Particle Image Velocimetry

Okeoghene Eboibi, Jonathan Edwards, Robert Howell, Louis Angelo Danao, *Member, IAENG*

***Abstract*— The vertical axis wind turbine aerodynamics are highly complex and unsteady. Inherent in the operation of VAWTs is the presence of the dynamic stall phenomenon that has a major influence in the overall performance of the rotor. The acquisition of a reliable experimental flow field data set presents a means to increase the level of understanding of VAWT performance and flow physics through visualisations. Particle image velocimetry (PIV) is a widely accepted technique employed in the measurement of the velocity flow fields in a vast array of fluid applications. The method developed in this study includes the setup of the PIV system in the wind tunnel, surface treatment of the VAWT blades, verification of test settings, and image processing and data analysis. The measurement of the flow fields around a VAWT blade at tip speed ratios of λ = 2.5 and 4 were carried out and the results show significant differences in the stalling characteristics between different λ with increased occurrence of deep and prolonged separation of flow from the blade surface at lower λ. In both cases, however, dynamic stall is observed. The data acquired is an invaluable reference for VAWT flow physics as well as validation of numerical models such as CFD.**

***Index Terms*— particle image velocimetry, vertical axis wind turbine, visualizations.**

I. Introduction

First attempts to study the flow physics around VAWT blades were performed in water by Fujisawa and Takeuchi [1] followed by Fujisawa and Shibuya [2]. In both studies, the flow field was visualised by a tracer method with plastic microspheres of 30–50μm diameter. The VAWT had a single straight blade of a NACA0018 section with chord c = 0.01m, span L = 0.135m, and rotor radius R = 0.03m and made of acrylic resin. The blade was fixed on an end plate with no central shaft to facilitate visualisation all around the rotation. The experiment was carried out in water tunnels with maximum flow velocity U = 0.05m/s giving a Reynolds number Re = 2,000. The light source was a set of stroboscopes triggered by a photosensor connected to the rotating end plate. The time interval between the two flashes was set to 2 or 3ms depending on the λ being tested.

Simao Ferreira et al [3-6] conducted PIV experiments on a larger VAWT in a wind tunnel. The work was performed at Re = 5×10^5 and 7×10^5 and λ = 2, 3, and 4. The flow was seeded using a fog machine with approximately 1μm droplets. The particles were illuminated using a light sheet generated by a Nd:YAG laser (200mJ/pulse) that was approximately 2mm thick at the field of view (FOV). A narrowband green filter was used for daylight interference on a CCD camera with 1,374 × 1,040 pixels. The time interval between pulses was set to roughly 8–pixel displacement of particles within a 32 × 32 pixel interrogation window assuming local velocities are 4 times the free stream values. At each selected blade position around the rotation, 30 to 100 images were taken and analysed with an iterative multi–grid window deformation technique.

This paper builds up on the previous studies and presents an advanced and very detailed methodology for PIV visualisation of the near-blade flow field of a VAWT. The methodology was originally developed by Edwards, through his PhD study [7] and used to validate a CFD model [8]. Danao et al. subsequently used the visualisations in their studies of VAWT performance in unsteady wind [9-11]. Most recently, Eboibi utilised and advanced the methods for his investigations into the effect of chord and solidity on VAWT performance [12]. A collected account of the authors' methodologies is presented here, in high detail. This paper is envisaged as being of significant interest, and of substantial practical use, to the VAWT experimenter.

II. Methodology

The rotor used was a straight–bladed VAWT with three NACA0022 blades of c = 0.04m each supported by two NACA0026 spokes of c = 0.03m at 25% and 75% blade length positions. The rotor R is 0.35m and L is 0.6m giving the VAWT a solidity of σ = 0.34 following the conventional definition (σ = Nc/R) and a wind tunnel blockage ratio of 0.29 (2RL/A, where A: test section area).

Manuscript received March 14, 2014. This work was supported by the Tertiary Education Trust Fund, the Delta State Polytechnics, Ozoro, Nigeria and the Engineering Research and Development for Technology, DOST, Philippines.

O. Eboibi, Ph.D. is a Lecturer at the Department of Agricultural Engineering, Delta State Polytechnics, Ozoro, Nigeria (e-mail: o.eboibi@gmail.com).

J. Edwards, Ph.D. is a Research Associate at the Department of Civil and Structural Engineering, University of Sheffield, Sheffield, U.K. (email: j.m.edwards@sheffield.ac.uk).

R. Howell, Ph.D. is a Lecturer at the Department of Mechanical Engineering, University of Sheffield, Sheffield, U.K. (email: r.howell@sheffield.ac.uk).

L. A. Danao, Ph.D. is an Assistant Professor at the Department of Mechanical Engineering, University of the Philippines, Quezon City, Philippines (corresponding author, email: louisdanao@coe.upd.edu.ph).

ISBN: 978-988-19253-5-0
ISSN: 2078-0958 (Print); ISSN: 2078-0966 (Online)

A. Particle Image Velocimetry

The basic principle of particle image velocimetry (PIV) is to capture a pair of images of the flow under study with a specific time interval between them. Each image is generated by seeding the fluid domain with particles that are assumed to follow the flow dynamics and illuminating a plane of particles using some sort of light source such as a laser sheet. The measured small difference in particle positions between images is used to compute for the velocity flow field.

A Dantec Dynamics 2D PIV system was used for all visualisation tests. The system has a Litron Nano–S–65 Nd:YAG laser which emitted light with a maximum energy of 65mJ per pulse at a wavelength of 520nm. A 4 megapixel CCD camera was used to capture the images. A TSI 9306A Six Jet Atomiser generated tracer particles of olive oil that had an approximate size of 2μm in diameter.

In PIV, particle motion is the measured quantity and is used to represent the fluid velocity field. Therefore, it is extremely important that the particles' tendency to attain velocity equilibrium with the fluid is achieved and can be properly quantified. The ability of tracer particles to follow the flow is measured using Stokes number S_k such that a value << 0.1 gives a tracing error of less than 1% [7, 13]. S_k is defined via Eq. (1).

$$S_k = \frac{\tau U}{d_c} \tag{1}$$

$$\tau = \frac{\rho_d d_d^2}{18\mu_f} \tag{2}$$

where τ: response time of the particle
U: velocity of the fluid under study
d_c: characteristic dimension of the obstacle
ρ_d: density of the tracer particle
d_d: diameter of the tracer particle
μ_f: dynamic viscosity of the fluid

The response time τ of the tracer particle should be faster than the smallest time scale of the flow and can be deduced using Eq. (2). In this study, olive oil (density ≈ 920kg/m^3) was used as tracer particle. The τ was computed to be about 1.1×10^{-5}. The characteristic dimension used was the chord length of the blade while the velocity of the fluid was set to U = 40m/s derived from the maximum computed local velocity of a comparable CFD simulation at $\lambda = 4$. These values led to a $S_k \approx 0.01$ which meant that the particles should follow fluid streamlines closely and avoid deviating from the flow during rapid changes in flow speed and direction.

Seeding was carried out by running the wind tunnel fan while introducing the particles upstream essentially seeding the entire laboratory room. This was found to be the most effective way to achieve adequate and uniform seeding distribution and density. After every 30 minutes of testing, the seeding was topped–up for 1 minute. The laser was mounted on an elevated platform outside the wind tunnel. The laser sheet plane was positioned midway between the support arm and the blade end, avoiding these disturbances to the blade flowfield. This was selected to be within the region that best represented a quasi–2D flow that can be compared to CFD results, yet avoided the support arm obscuring the most critical part of the flowfield.

B. Experimental Setup

The setup of the equipment for the PIV campaign is shown in Fig. 1. A camera rig was installed on top of the wind tunnel to capture the end view of the blade perpendicular to the laser sheet plane while a 3000 pulse per rev encoder was mounted at the bottom to measure rotational velocity of the rotor. The camera was mounted on a rotating arm with the axis in line to the VAWT axis thereby permitting the positioning of the FOV to the desired azimuth, the position of a blade around the rotor. The synchronisation of the laser and the camera with the desired azimuth was achieved using an extra channel in the encoder that gave a once–per–rev pulse. The camera and the laser are perpendicular relative to each other and to the general direction of flow.

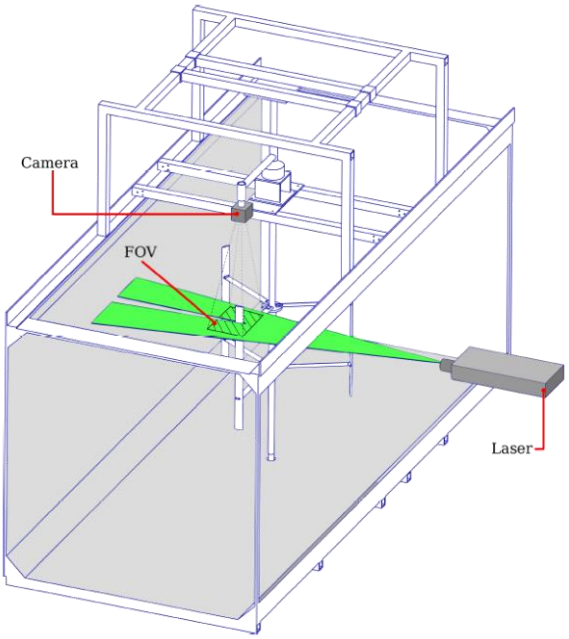

Fig. 1. The experiment setup showing the position of the laser sheet relative to the camera and the blade, and the location of the FOV.

C. Image Processing

A sample of one of an acquired raw image pair is presented in Fig. 2. It shows the 2048 × 2048 pixel FOV with an approximate area of 135mm × 135mm. Also shown are the flow direction, seeded particles, blade surface reflection, support arm and shadow region. Prior to processing the data, the acquired images were masked to remove areas in the raw image that were unwanted. It was necessary to remove these regions, such as near blade surface reflection and shadow region, since the vectors within these regions could be poorly correlated when processed without being masked out.

ISBN: 978-988-19253-5-0
ISSN: 2078-0958 (Print); ISSN: 2078-0966 (Online)

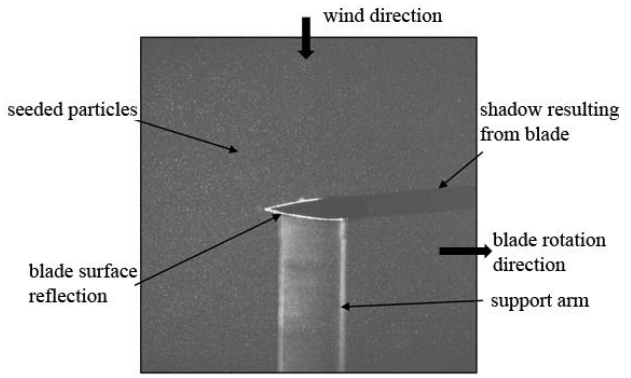

Fig. 2. Raw PIV data at a 90° azimuth and U = 6m/s.

The captured image was split into interrogation windows and processed using cross correlation. To determine the velocity vector for each interrogation window, basic cross correlation function, which relates pixel intensity with particle distance, was used. The displacement with the highest correlation is the most likely particle movement within the interrogation window. The process was applied to the entire image and the output is shown in Fig. 3.

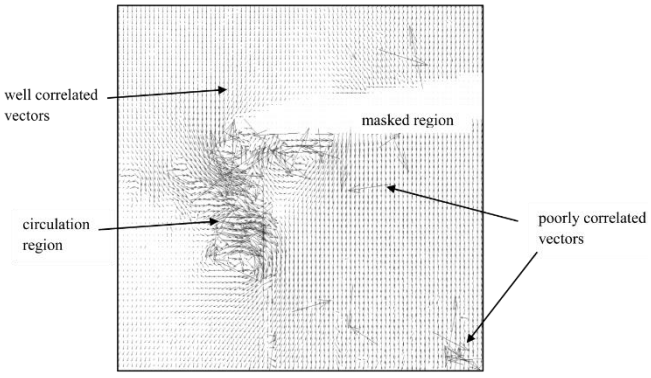

Fig. 3. Result of cross-correlation procedure on acquired data.

To remove poorly correlated vectors, a moving average filter with a 3 × 3 window was applied on the cross-correlated images. The moving average filter compares a velocity vector against surrounding vectors and replaces vectors with magnitudes exceeding 20% of the neighbouring vectors. As the edge of an image is slightly further away from the camera aperture than the centre, the flow velocity scaling factor is not constant. However, in the case of the measurements detailed in this study the camera and FOV were 0.9m apart, resulting in a negiligble difference of only 0.3% between the scaling factor for the centre and edge of the image.

Multiple image pairs were ensemble averaged to get a representative picture of the velocity flow field for each azimuth position (Fig. 4). The number of image pairs captured for each azimuth position was determined after a systematic study of the effects of sample number on the ensemble averaged velocity plot. It was determined that beyond 50 image pairs there was little observed difference in the velocity plots and 50 was a sufficient number for the author's study of fundamental flow physics. It must be stressed however, that for future investigations, the number of image pairs should be reassessed for significantly different rotors or operating conditions, or for studies with more in-depth scope.

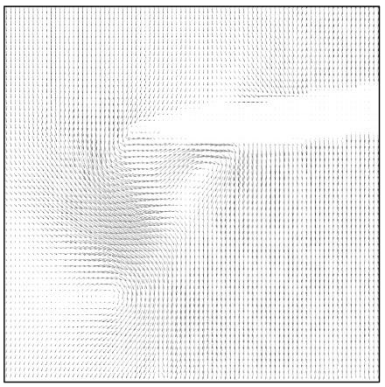

Fig. 4. Ensemble averaged velocity flow field for 90° azimuth.

D. Blade Surface Treatment

Surface reflection from the blades due to the laser was unavoidable and had to be minimized. The intensity of emitted light from the laser and the image filtering devices used to limit these effects are a major consideration during PIV experiments. Despite the optimal camera position and laser intensity, surface reflection was still present in the images. Hence, it was necessary to treat the blade surface to achieve a tolerable level of reflection to prevent damage to the camera CCD and reduced the negative effects on the accuracy of the results.

The VAWT blades are aluminium and naturally have highly reflective surfaces even at very low laser intensity. In order to reduce the surface reflection in the current study, the blade surface was treated following the procedure detailed in [14]. A thin layer of body filler was applied to the surface of the blade and allowed to dry for about 2 hours. The body filler was then sanded with a #200 grit sandpaper, thereafter, a thin layer of matt black was sprayed on the surface of the blade. The blade was allowed to dry for several hours and inspected using a small microscope to ascertain the uniformity of the applied matt black. Upon satisfactory results, and in addition to the coat of the matte black paint, a thin layer of Dykem steel red paint was applied and allowed to dry for several hours. The Dykem steel red paint is suitable because it contains Rhodamine which absorbs wavelengths of light close to 520nm, the wavelength of the laser used in this investigation.

E. Seeding Concentration

The correct seeding density is important in capturing complicated flow details especially in the recirculation or separation zones. To achieve this, seeding must be uniformly distributed and of the required concentration. The atomizer was run from 5 to 10 minutes at intervals of 1 minute. The data were analysed based on the correlated vectors.

Fig. 5 shows the effects of varying the seeding time on the rejected vectors. At the lowest seeding time of 5 minutes, 4.1% of the vectors were poorly correlated, above the 3% tolerable level. As seeding time is increased, a reduction in poorly correlated vectors is observed. As seen in the figure, 3.0% of vectors are rejected at 8 minutes seeding while 2.6% of vectors are rejected at 10 minutes seeding time. In consideration of time and small differences between the poorly correlated vectors between 8 and 10 minutes, 8 minutes seeding time was adopted for all the PIV testing presented in this study.

ISBN: 978-988-19253-5-0
ISSN: 2078-0958 (Print); ISSN: 2078-0966 (Online)

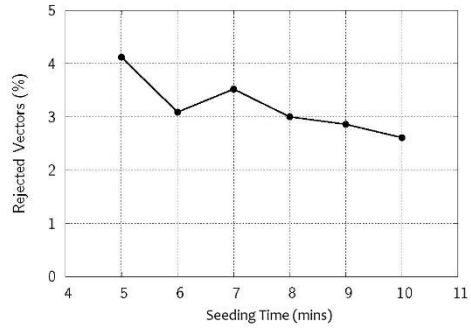

Fig. 5. The effects of seeding time on percentage of rejected vectors.

F. Laser Power

The intensity of the light sheet is directly related to the laser power. At the maximum laser power, the laser can emit highly concentrated light beams. For safety reasons, and also to prevent the camera sensors from being damaged due to too high light sheet intensity, different levels of the laser power were tested to find a suitable power level. Images were acquired from 70% - 100% of the laser power at 10% intervals – starting from low to high, for safety.

The data were analysed based on the quality of the correlation. Fig. 6 shows the percentage of poorly correlated vectors for 70% power level at above 20%. At 80% laser power level, poorly correlated vectors drop to 6%. Further reduction in rejected vectors is observed as laser power is increased to 90% and 100%. There is very small difference in percentage of rejected vectors between 90% and 100% laser power. The 90% laser power level is adopted for this study since the rejected vectors are less than 3%.

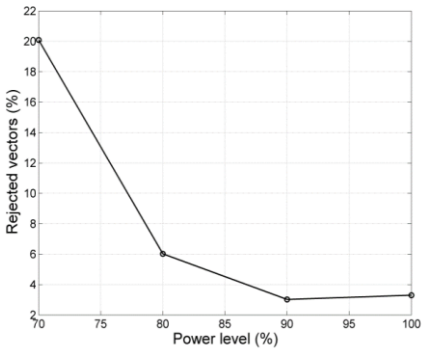

Fig. 6. The effects of laser power level on percentage of rejected vectors.

G. Time Between Pulses

The time interval between image acquisitions is a critical parameter because there must be sufficient movement of the tracer particle within the interrogation window to accurately represent the flow velocity. Too short intervals would result in inaccurate particle displacement computations while too long intervals may result in particles having exited the window altogether. The time interval was varied from 5μs to 150μs. The poorly correlated vectors at 150μs constitute 57% of all vectors in the FOV (Fig. 7). The high number of rejected vectors is due to the particles that have already exited the window in the second image or new particles have entered into the window in the second image.

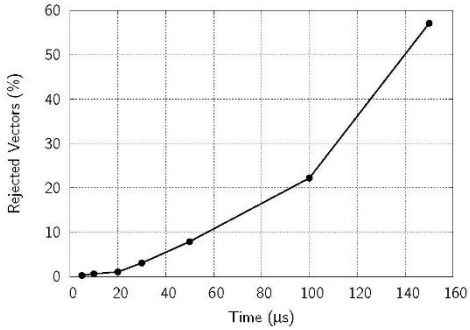

Fig. 7. The effect of time between laser pulses on percentage of rejected vectors.

At 50μs, the number poorly correlated vectors correspond to 8% of rejected vectors. Low levels of poorly correlated vectors are observed at 5μs, 10μs and at 20μs time intervals, with rejected vectors at 3% or lower. For this study 20μs was chosen for the PIV testing.

III. Results and Discussion

One of the major characteristics of VAWT aerodynamics is the dynamic stall phenomenon that is usually expected in a broad range of operating conditions. When an aerofoil is under oscillating motion in a moving fluid, stalling can be considerably delayed beyond the static stall angle. A consequence of this is that static aerofoil analysis and data are no longer suitable because the forces on the blade exceed static stall values and large hysteresis are exhibited with respect to the instantaneous angle of attack. This is more prominent in oscillations with amplitudes in the order of the static stall angle [15]. Dynamic stall is characterised by the shedding of a vortex over the suction surface of an aerofoil under pitching motion in a stream of fluid. If the frequency, amplitude and maximum incidence are sufficiently high, an organised and clearly defined shedding of vortices is observed. Necessary to the analysis of VAWT performance is the proper understanding of the onset of blade stall including the dynamic stall and the subsequent reattachment of flow.

During operation, a VAWT blade experiences cyclic variations in angle of attack α. The blade may undergo stalled and unstalled conditions as well as interact with its own wake and that of other blades within one rotation. As the VAWT rotates with angular velocity ω in a flow of wind speed U, the angle of attack α varies periodically between positive and negative values. The magnitude of the angle of attack is given by

$$\alpha = \tan^{-1}\left(\frac{\sin\theta}{\lambda + \cos\theta}\right) \tag{3}$$

where θ is the azimuth angle and λ is the tip speed ratio. The variation of α resembles a skewed sine wave as shown in Fig. 8. This perceived variation is relative to a reference frame attached to the rotating VAWT with its origin at the VAWT axis. As the tip speed ratio λ increases, the skewness of the α-variation reduces and the profile comes closer to a sine wave (zero skew).

ISBN: 978-988-19253-5-0
ISSN: 2078-0958 (Print); ISSN: 2078-0966 (Online)

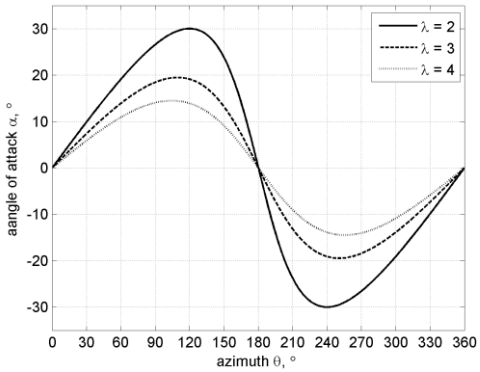

Fig. 8. Variation of angle of attack α at different tip speed ratios λ.

A major objective of this study is to make available the stalling characteristics of VAWT blades at two different tip speed ratios through visualisations. The velocity flow field acquired in the PIV campaign does not provide very meaningful information due to difficulties in interpretation and identification of separation and stalled flow. To make more sense of the results, the velocity data was further processed to produce vorticity plots. Vorticity has been chosen since it shows a good indication of separation and reattachment, wake convection and interaction, and presence of shed vortices without the use of streamlines, which can be messy at times. Vorticity is defined as the curl of the velocity field. In two dimensions such as in 2D PIV, it is expressed through Eq. (4).

$$\Phi_z = \frac{\partial V}{\partial x} - \frac{\partial U}{\partial y} \tag{4}$$

Fig. 9 shows the vorticity plot of 90° azimuth position. It can be seen that the suction side of the aerofoil is fully separated with a pair of vortices being shed. Red contours indicate anti-clockwise vorticity while blue contours show clockwise vorticity. There are spurious vorticity contours next to the shadow region that does not have velocity data and along the support arm edge that has strong laser light reflection. These are ignored in the analysis.

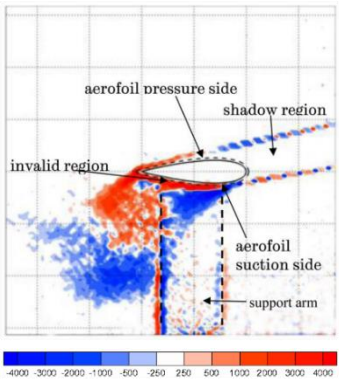

Fig. 9. Vorticity plot at U = 6m/s, λ = 2.5 and θ = 90°.

A. *Flow Field at λ = 2.5*

Fig. 10 shows the vorticity contours for different azimuth positions at U = 6m/s and λ = 2.5. It was observed that the flow is fully attached from the start of rotation up to θ = 60° (Fig. 10a). At these conditions, classical static aerofoil studies dictate the angle of attack perceived by the blade to have exceeded static stall already ($\alpha_{stall} \approx 11°$) [11]. This is a good indication of the onset of dynamic stall. At θ = 70° (Fig. 10b), the growth of a leading edge vortex (LEV) is initiated and is seen to continue to develop until it fully forms and starts to detach from the blade (Fig. 10c). Following this, another vortex forms at the trailing edge (TEV) that facilitates the detachment of the LEV (Fig. 10d) and itself is detached from the blade surface (Fig. 10e). The process of the alternate shedding of vortices akin to the Kármán Vortex Street occurs until the separation depth starts to shallow out and the blade stall reduces due to the decrease of the perceived angle of attack. At Fig. 10f, blade stall is still deep with the separation point still within quarter chord from the leading edge. Once again, classical static aerofoil theory suggests that the angle of attack at this condition is below stall and the flow should be fully attached by this time. On the contrary, full reattachment only happens after θ = 190° (not shown) which is way past the halfway point in a full rotor revolution, at which α would be expected to be zero.

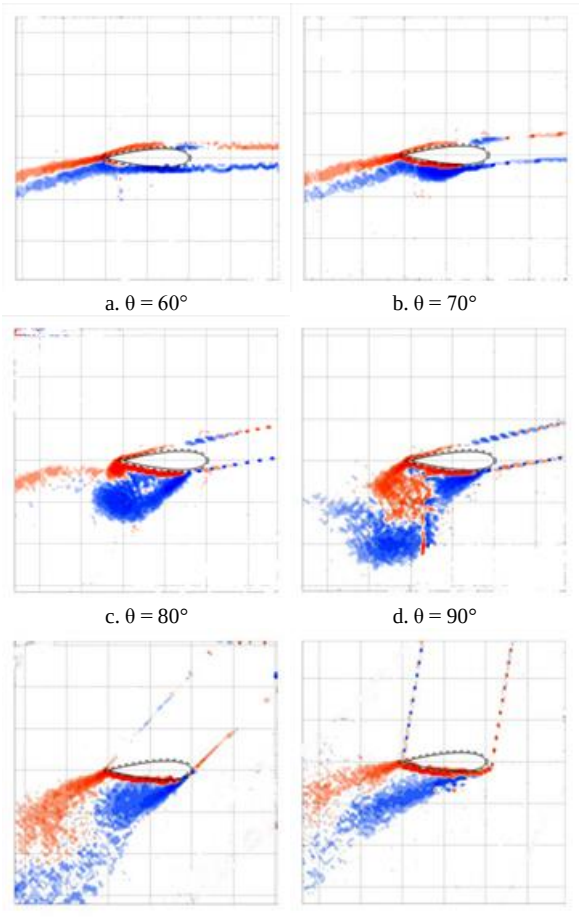

a. θ = 60° b. θ = 70°
c. θ = 80° d. θ = 90°
e. θ = 100° f. θ = 170°

Fig. 10. Visualisations of vorticity at U = at 6m/s and λ = 2.5.

B. *Flow Field at λ = 4.0*

The delay in the stalling of the blade is also observed at λ = 4.0. Fully attached flow is seen up to azimuth angles θ = 120° (Fig. 11a). Similarly, the perceived α at this azimuth should be greater than static stall conditions. This suggests that the blade is undergoing dynamic stall even at high λ. Separation is initiated not from the leading edge but from the trailing edge and full separation bubble is observed at θ = 130° (Fig. 11b) that progressively bursts into fully separated flow at θ = 140° (Fig. 11c). A very small trailing

ISBN: 978-988-19253-5-0
ISSN: 2078-0958 (Print); ISSN: 2078-0966 (Online)

edge roll up is observed but does not develop into a chord-sized vortex as seen at lower λ. Delayed reattachment is also seen at this λ with partial separation still persistent at θ = 170° (Fig. 11d) where the expected α should be less than 5°.

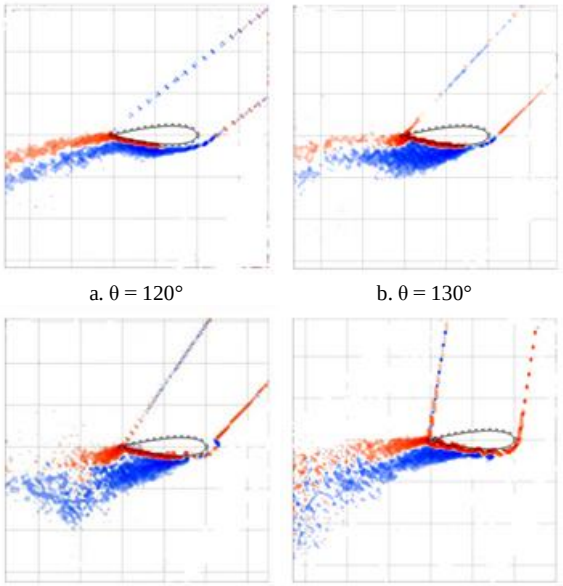

a. θ = 120° b. θ = 130°

c. θ = 140° d. θ = 170°

Fig. 11. Visualisations of vorticity at U = at 6m/s and λ = 4.0.

IV. Conclusions

A method has been developed and presented in the acquisition of visualization data for VAWT blade aerodynamics through Particle Image Velocimetry. A systematic characterization of parameters was carried out to establish the appropriate settings in the conduct of experiments including seeding concentration, laser intensity, and time interval. Results show the presence of dynamic stall at two different operating conditions with significant delay in the onset of stall and reattachment. This study provides valuable information relevant to the study of stall influenced VAWT performance as well as validation data for computational modelling work.

Nomenclature

A	rotor swept area
c	blade chord
d_c	obstacle characteristic dimension
d_d	tracer particle diameter
L	blade span
R	rotor radius
Re	Reynolds number
U	flow velocity
S_k	Stokes number
CFD	Computational Fluid Dynamics
FOV	field of view
LEV	leading edge vortex
PIV	Particle Image Velocimetry
TEV	trailing edge vortex
VAWT	vertical axis wind turbine
α	angle of attack
θ	azimuth position
λ	tip speed ratio
μ_f	dynamic viscosity of the fluid
ρ_d	tracer particle density
σ	solidity
τ	tracer particle response time
Φ_z	Z-vorticity

References

[1] Fujisawa, N., and Takeuchi, M., 1999, "Flow Visualization and Piv Measurement of Flow Field around a Darrieus Rotor in Dynamic Stall," Journal of Visualization, 1(4), pp. 379-386.

[2] Fujisawa, N., and Shibuya, S., 2000, "Observations of Dynamic Stall on Darrieus Wind Turbine Blades," Journal of Wind Engineering and Industrial Aerodynamics, 89(2001)(pp. 201-214.

[3] Simão Ferreira, C. J., Dixon, K., Hofemann, C., Van Kuik, G., and Van Brussel, G. J. W., 2009, "The Vawt in Skew: Stereo-Piv and Vortex Modeling," AIAA 2009-1219, 47th AIAA Aerospace Sciences Meeting, Orlando, Florida, USA.

[4] Simão Ferreira, C. J., Van Brussel, G. J. W., Scarano, F., and Van Kuik, G., 2008, "Piv Visualization of Dynamic Stall Vawt and Blade Load Determination," 46th AIAA Aerospace Sciences Meeting and Exhibit, Reno, Nevada, USA.

[5] Simão Ferreira, C. J., Van Kuik, G., Van Brussel, G. J. W., and Scarano, F., 2009, "Visualization by Piv of Dynamic Stall on a Vertical Axis Wind Turbine," Experiments in Fluids, 46(1), pp. 97-108.

[6] Simão Ferreira, C. J., Van Zuijlen, A., Bijl, H., Van Bussel, G., and Van Kuik, G., 2010, "Simulating Dynamic Stall in a Two-Dimensional Vertical-Axis Wind Turbine: Verification and Validation with Particle Image Velocimetry Data," Wind Energy, 13(1), pp. 1-17.

[7] Edwards, J., 2012, "The Influence of Aerodynamic Stall on the Performance of Vawt Blades," PhD thesis, University of Sheffield, Sheffield, UK.

[8] Edwards, J. M., Danao, L. A., and Howell, R. J., 2012, "Novel Experimental Power Curve Determination and Computational Methods for the Performance Analysis of Vertical Axis Wind Turbines," Journal of Solar Energy Engineering, 134(3), pp. 11.

[9] Danao, L. A., Edwards, J., Eboibi, O., and Howell, R., 2013, "A Numerical Investigation into the Effects of Fluctuating Wind on the Performance of a Small Scale Vertical Axis Wind Turbine," Engineering Letters, 21(3), pp. 149-157.

[10] Danao, L. A., Edwards, J., Eboibi, O., and Howell, R., 2014, "A Numerical Investigation into the Influence of Unsteady Wind on the Performance and Aerodynamics of a Vertical Axis Wind Turbine," Applied Energy, 116(0), pp. 111-124.

[11] Danao, L. a. M., 2012, "The Influence of Unsteady Wind on the Performance and Aerodynamics of Vertical Axis Wind Turbines," PhD thesis, University of Sheffield, Sheffield, UK.

[12] Eboibi, O., 2013, "The Influence of Blade Chord on the Aerodynamics and Performance of Vertical Axis Wind Turbines," PhD thesis, University of Sheffield, Sheffield, UK.

[13] Raffel, M., Willert, C. E., Wereley, S. T., and Kompenhans, J., 2007, *Particle Image Velocimetry: A Practical Guide*, Springer Berlin Heidelberg,

[14] Pierce, A., and Lu, F., 2011, "New Seeding and Surface Treatment Methods for Particle Image Velocimetry," 49th AIAA Aerospace Sciences Meeting including the New Horizons Forum and Aerospace Exposition,

[15] Mccroskey, W. J., 1981, "The Phenomenon of Dynamic Stall," Technical Report No. NASA TM-81264, Ames Research Center, Moffett Field, California.

ISBN: 978-988-19253-5-0
ISSN: 2078-0958 (Print); ISSN: 2078-0966 (Online)